Heliyon 10 (2024) e39874

Contents lists available at ScienceDirect

Heliyon

journal homepage: www.cell.com/heliyon

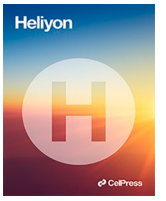

Research article

Total glucosides of Picrorhizae Rhizome alleviate non-alcoholic steatohepatitis (NASH) by specifically targeting acyl-CoA oxidase 1

Fang-Fang Zhuo [a], Xiao-Qing Li [b], Jun Zhang [b], Fu-Ming Zhang [b], Zhao-Hui Song [b], Yi He [b], Li Ding [d], Dan Liu [c], Peng-Fei Tu [a,*], Xiao-Hui Ma [b,**], Ke-Wu Zeng [a,***]

[a] State Key Laboratory of Natural and Biomimetic Drugs, School of Pharmaceutical Sciences, Peking University, Beijing, 100191, China
[b] National Key Laboratory of Chinese Medicine Modernization, Tasly Academy, Tasly Pharmaceutical Group Co., Ltd., Tianjin, 300410, China
[c] Proteomics Laboratory, Medical and Healthy Analytical Center, Peking University Health Science Center, Beijing, 100191, China
[d] School of Chinese Materia Medica, Tianjin University of Traditional Chinese Medicine, Tianjin, 301617, China

ARTICLE INFO

Keywords:
Nonalcoholic steatohepatitis (NASH)
Total glucosides of Picrorhizae Rhizome
Target identification
Acyl-CoA oxidase 1 (Acox1)
Fatty acids

ABSTRACT

Nonalcoholic steatohepatitis (NASH), a chronic liver disease characterized by the accumulation of fat in the liver, is highly prevalent on a global scale. In this study, we investigated the effects of total glucosides of Picrorhizae Rhizome (TGPR), the primary active ingredients in traditional Chinese herbal medicine derived from *Picrorhiza scrophulariiflora* Pennell. TGPR is known for its efficiency in attenuating NASH, in mouse models induced by methionine-choline deficient (MCD) diet or high-fat diet (HFD). Our findings indicated that TGPR exhibited efficacy in reducing hepatic steatosis and lowering serum lipid levels, specifically triglyceride and total cholesterol in the NASH model. Meanwhile, TGPR exhibited a suppressive effect on the production of pro-inflammatory cytokines. Mechanistically, we identified acyl-CoA oxidase 1 (Acox1) as a crucial cellular target of TGPR, influencing lipid metabolism and ATP production to treat NASH. Additionally, we found that the major components of TGPR, including Picroside I, Picroside II, and Picroside IV, exhibit significant binding abilities to the target Acox1 at its catalytic C-terminal α-domain, stabilizing its protein expression. TGPR binding to Acox1 facilitated the degradation of fatty acids via the Acox1-mediated MAPK signaling pathways, and consequently plays a role in regulating energy metabolism and reducing liver inflammation. In summary, our study demonstrates that TGPR effectively counteracts NASH by specifically targeting Acox1, thereby providing a significant clinical solution for the treatment of NASH.

1. Introduction

Nonalcoholic fatty liver disease (NAFLD) is a highly prevalent chronic liver condition affecting individuals globally, encompassing a spectrum from simple steatosis to nonalcoholic steatohepatitis (NASH) [1]. NASH is commonly associated with obesity, insulin resistance, and metabolic syndrome, and can progress to more severe forms of liver disease such as fibrosis, cirrhosis and

* Corresponding author.
** Corresponding author.
*** Corresponding author.
E-mail addresses: pengfeitu@bjmu.edu.cn (P.-F. Tu), maxiaohui@tasly.com (X.-H. Ma), ZKW@bjmu.edu.cn (K.-W. Zeng).

https://doi.org/10.1016/j.heliyon.2024.e39874
Received 10 April 2024; Received in revised form 11 October 2024; Accepted 25 October 2024
Available online 26 October 2024

hepatocellular carcinoma [2]. Recognized as the progressive form of NAFLD, NASH is identifiable by the presence of steatosis, characterized by the accumulation of fat deposits as well as inflammation [3]. Excessive lipids in the liver lead to lipotoxicity, oxidative stress, and inflammation, contributing to liver damage and the progression of NASH [3]. Thus, targeting lipid metabolism pathways and inflammation may effectively treat fatty liver disease. However, the current treatment options for NASH remain limited due to the absence of approved effective pharmacological therapies specifically designed for NASH [4]. Therefore, there is a critical need for the development of innovative therapeutic agents to effectively manage NASH.

Acyl-CoA oxidase 1 (Acox1) is a critical rate-limiting enzyme which catalyzes the desaturation of very-long-chain acyl-CoAs to 2-trans-enoyl-CoAs [5]. This enzymatic reaction is essential for the subsequent processes of β-oxidation and energy production from fatty acids. Previous reports have indicated an association between Acox1 and spontaneous liver damage in humans [6,7]. Meanwhile, mice with Acox1 deficiency exhibit hepatic metabolic derangements, resulting in the development of steatohepatitis and subsequent hepatic carcinomas [8]. In particular, the function of Acox1 in NAFLD has recently been uncovered, encompassing its role in promoting oxidative damage and inducing dysfunction in lipid metabolism [9,10]. Furthermore, Acox1 has been implicated in the dysregulation of fat metabolism and poor prognosis during the progression of NAFLD. Consequently, Acox1 has emerged as a promising therapeutic target for addressing NASH.

Picrorhiza scrophulariiflora Pennell, has been widely acknowledged as a traditional Chinese medicine that possesses therapeutic properties for inflammatory conditions such as arthritis and asthma [11]. Previous research has revealed that total glucosides of Picrorhizae Rhizome (TGPR) derived from *Picrorhiza scrophulariiflora* Pennell are composed of diversified active compounds, such as iridoids, phenylethanoids, glycosides, and triterpenoids [12,13]. Recent investigations have elucidated the diverse array of biological activities demonstrated by TGPR, encompassing anti-inflammatory, anti-nociceptive, antioxidative, and hepatoprotective properties [14,15]. However, there is still a need for a comprehensive understanding of the underlying mechanisms by which TGPR confers its protective effects against NASH. In particular, the identification of specific cellular targets of TGPR remains uncertain.

In this study, we utilized an MCD (methionine-choline-deficient) diet-induced steatohepatitis model in C57BL/6J mice, which resembles the liver disease observed in humans with NASH. Subsequently, we investigated the therapeutic effects of TGPR on NASH and elucidated the underlying mechanisms. Notably, we prepared TGPR-crosslinked nanoparticles to explore cellular targets through an affinity purification strategy. Upon employing dimethyl labeling quantitative proteomics [16,17], we were able to successfully identify Acox1 as a significant target protein. Mechanistically, we have uncovered that TGPR has the ability to enhance the stability of Acox1 protein, resulting in a suppressed inflammatory response in the liver. Furthermore, TGPR targets Acox1 to enhance fatty acid oxidation by repressing the MAPK signaling axis. Collectively, our studies provide valuable insights into the potential of TGPR as a therapeutic intervention for attenuating NASH and offer a comprehensive understanding of the molecular signaling mechanisms of Acox1-regulated NASH.

2. Materials and methods

2.1. Preparation of TGPR

Total glucosides of Picrorhizae Rhizome (TGPR) used in this study was obtained from Tasly Pharmaceutical Group Co., Ltd. (Tianjin, China) with a lot number of 20211102. The quality of TGPR was confirmed by Tianjin University of Traditional Chinese Medicine. TGPR (lot: 20211102) was dissolved in normal saline to prepare the TGPR solution for animal experiments. TGPR (lot: 20211102) is extracted from the medicinal herb *Picrorhiza scrophulariiflora* Pennell (lot: 20191001), both stored at Tasly Pharmaceutical Group Co., Ltd.

2.2. Identification of TGPR components with HPLC

The Luna C18-reversed phase analytical column (Torrance, CA, USA) was applied. The sample was separated using a linear gradient of mobile phase, consisting of 15.5 % acetonitrile and 84.5 % glacial acetic acid aqueous solution (0.5 % v/v), with a flow rate set at 1.0 mL/min. The instrument was configured to detect signals at a wavelength of 275 nm. Under this chromatographic condition, the separation of each peak was greater than 1.5. A consistent injection volume of 10 μL was utilized for each run. Then, methanol was fixed to prepare a standard solution of Piceoside (2 μg/mL), Vanillic acid (4 μg/mL), Androsin (8 μg/mL), Picroside I (40 μg/mL), Picroside II (120 μg/mL), Picroside III (20 μg/mL), Picroside IV (40 μg/mL), Verminoside (12 μg/mL) and 6-feruloylcatalpol (8 μg/mL). The concentration of the TGPR sample solution used for detection was prepared at 400 μg/mL.

2.3. MCD-induced NASH model

The ethical approval for all animal procedures conducted in this study was obtained from the Institutional Animal Care and Use Committee at Peking University (License No. LA2022200). After being purchased from VITAL RIVER Laboratories (Beijing, China), six-week-old male C57BL/6J mice were acclimated to a 12-h light/dark cycle with ad libitum access to food and water. Following this acclimatization period, the mice were divided into three groups (n = 10 each) and fed different diets. Control group: Mice were fed with normal chow (10 % fat). MCD group: Mice were fed with MCD diet (10 % fat, 0 % methionine, 0 % choline). TGPR group: Mice were fed with MCD diet (10 % fat, 0 % methionine, 0 % choline). After a 4-week period of being fed with MCD, the TGPR group received a daily intragastric administration of TGPR (36.2 mg/kg) for an additional 5 weeks. The dose design of TGPR is based on the high dose used in the phase II clinical trial with registration number CTR 20222042. Specifically, participants in the Phase II clinical

study of Picrorhizoside capsules received 10 capsules per person per day, each containing 26.47 mg of Picrorhizoside, resulting in a total daily intake of 264.7 mg per person. The equivalent dose for mice was calculated to be 34.4 mg/kg. The safe dose of TGPR for combined early comprehensive treatment is 50 mg/kg. Ultimately, we selected a therapeutic dose of 36.2 mg/kg for the MCD-fed mice.

2.4. Hematoxylin & eosin (H&E) and immunohistochemistry (IHC)

Liver tissues were fixed in 4 % buffered formalin, dehydrated, and embedded in paraffin. 4-μm sections of tissue specimens were obtained for H&E and IHC staining. For H&E staining, the sections would typically be stained with hematoxylin to label cell nuclei and eosin to provide contrast and color to the other structures in the tissue. The NAS score was calculated by summing the scores of steatoses, lobular inflammation, and hepatocyte ballooning observed in the H&E-stained liver sections. The NAS scoring index comprised steatosis (0–3), lobular inflammation (0–3), and hepatocyte ballooning (0–3). Immunohistochemistry staining involved labeling the sections with primary antibodies targeting TNF-α (60291-1-Ig), IL-6 (ab6672), IL-1β (ab283818), and Acox1 (10957-1-AP), along with suitable secondary antibodies. The images were visualized by Zhiyue WS-10 Digital Panoramic Scanner (Beijing, China) and immunohistochemical staining area was quantified by ImageJ.

2.5. Oil red O staining

To visualize lipid accumulation in frozen liver sections embedded in OCT, we performed staining using Oil Red O dye for a duration of 30 min. This was accomplished by diluting a 0.5 % stock solution in isopropanol with water at a ratio of 60:40 (v/v). Then, the tissue specimens were examined by Zhiyue WS-10 Digital Panoramic Scanner (Beijing, China).

2.6. Biochemical assay

Blood samples were collected from the mice following a 12 h fasting period. The obtained serum was analyzed for TG and TC, using the Chemwell BRED Analyzer (HITACHI, Tokyo, Japan). For the measurement of hepatic TC and TG, 100 mg of liver tissue was homogenized in 1 mL of isopropyl alcohol. The total cholesterol assay kit (BC1985) and triglyceride assay kit (BC0625) were purchased from Solarbio (Beijing, China).

2.7. Quantitative real-time polymerase chain reaction (RT-PCR)

Total RNA was isolated from mouse liver using the StarSpin Animal RNA Mini Kit Genstar (Beijing, China). RT-PCR was performed using Hieff qPCR SYBR Green Master Mix, manufactured by YEASEN (Beijing, China). All primer sequences were synthesized by Ruibo Biotech (Beijing, China), as shown in Table 1.

2.8. Identification of cellular targets using an affinity purification strategy

(1) Preparation of TGPR-crosslinked nanoparticles (TGPR-NPs). TGPR was chemically coupled onto Fe_3O_4 nanoparticles performed as previously described [19]. Briefly, $FeCl_3{\cdot}6H_2O$, Na_3Cit, and $NaAc{\cdot}3H_2O$ were dissolved in ethylene glycol and reacted at 200 °C for 8 h. After the addition of racemic-2,3-dimercaptosuccinic acid, sulfhydryl-bound Fe_3O_4 beads were synthesized. Subsequently, ethylester L-lysine triisocyanate and 4,4′-dihydroxybenzophenone were added to produce DHBP-bound Fe_3O_4 nanoparticles. TGPR (5 mg) was then added to 20 mL of methanol containing 4,4′-dihydroxybenzophenone-bound Fe_3O_4 nanoparticles. The mixture was subjected to UV irradiation (254−365 nm) for 60 min.
(2) Transmission electron microscope (TEM) analysis. TEM characterization was performed at an accelerating voltage of 80 kV utilizing the Tecnai G2 F20 microscope (Hillsboro, OR, USA).
(3) Pull-down assay. TGPR-NPs were mixed with MCD-induced NASH liver lysate and incubated at 4 °C for 4 h. During this time, an excess of free TGPR (100 μg/mL) was added to compete with TGPR-NPs for target proteins. After elution, the proteins captured by TGPR-NPs were analyzed using a nano-HPLC-tandem LTQOrbitrap Velos pro mass spectrometer (Thermo Fisher Scientific, Waltham, MA, USA).

Table 1
Sequences of primer used in this study.

Primers for qRT-PCR	5′ to 3′
TNF-α-F	GGACTAGCCAGGAGGGAGAA
TNF-α-R	CGCGGATCATGCTTTCTGTG
IL-6-F	GAGGGCCATTCGGATCATGT
IL-6-R	ATGTGCCCAATGGACAGGTT
IL-1β-F	TGCCACCTTTTGACAGTGATG
IL-1β-R	GGAGCCTGTAGTGCAGTTGT
Gapdh-F	GGTGAAGGTCGGTGTGAACG
Gapdh-R	CTCGCTCCTGGAAGATGGTG

2.9. Protein quantification based on stable isotope labeling by dimethylation

(1) Dimethylation labeling. Dimethylation labeling was performed by dissolving the peptides in NaH_2PO_4 (pH 6.0). Before utilization, a 4 % (v/v) formaldehyde solution was mixed with 1.2 M $NaBH_3CN$ in a proportion of 1:1 (v/v). Subsequently, 8 μL of the resulting mixture was introduced into the solution containing the peptides. The subsequent steps encompassed a quick mixing followed by centrifugation. The resultant mixture was then incubated at 30 °C for 1 h. The labeling reaction was ultimately halted by introducing 16 μL of a 1 % (v/v) solution of ammonia. The labeled products underwent additional purification and desalting using a Waters Sep-pak C18 column.

(2) LC-MS for target identification. The samples were loaded onto an Easy-column C18-A1 trap column with an online desalting wash. The separation was subsequently conducted on an EASY-nLC 1000 system, employing an Easy-column C18-A2 at a flow rate of 300 nL/min. The mobile phase consisted of phase A (0.1 % FA in water) and phase B (0.1 % FA in acetonitrile). The LC gradient comprising 2 %–40 % phase B, for 70 min, followed by 40 %–95 % phase B for 5 min and finally holding at 95 % phase B for 20 min. The software and instruments used in the described process are from Thermo Fisher Scientific (Waltham, MA, USA).

2.10. Molecular docking

The docking process utilized the Induced Fit Docking module of Schrodinger 2018. The crystal structure of the Acox1 protein (AF-Q15067-F1) was prepared using the Protein Preparation Wizard, which assigned bond orders, added hydrogen atoms, and removed water molecules. Subsequently, the protein was energy minimized with the OPLS3 force field. The receptor grid was generated using the Receptor Grid Generation module. Small molecules (Picroside I, Picroside II, and Picroside IV) were then docked with the protein using the Induced Fit Docking module, with Glide XP chosen for precision.

2.11. Cellular thermal shift assay (CETSA)

Total protein in NASH livers were extracted in RIPA buffer. The resulting lysates, with a concentration of 3.0 mg/mL, were divided

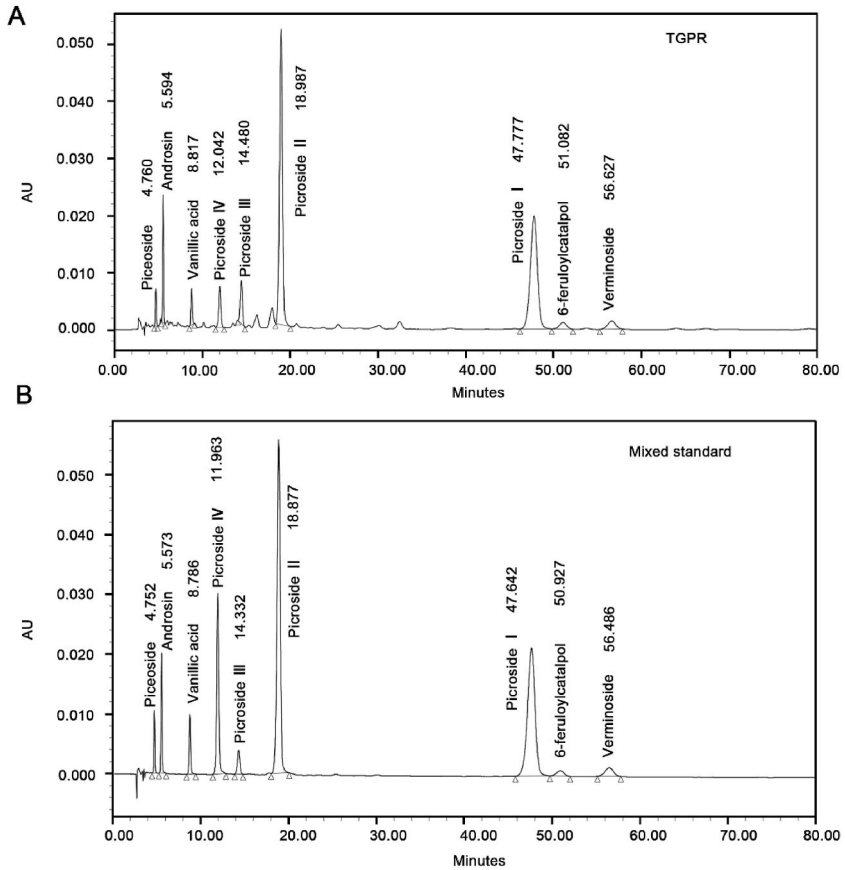

Fig. 1. Identification of TGPR constituents. HPLC profiles of TGPR (A) and mixed standard compounds (B).

into two aliquots. One aliquot was assigned as the control, whereas the other was exposed to TGPR (100 μg/mL) and subsequently incubated on a rotating platform at 4 °C for 1 h. The lysates were subjected to individual heating at specified temperatures (37, 40, 43, 46, 49, 52, 55, 58, 61, and 64 °C). The following procedures were carried out as previously described [20].

2.12. Western blotting

Total proteins in liver tissue were extracted in RIPA buffer and the protein concentration was determined using a BCA kit. The samples were then separated by 10 % SDS-PAGE, transferred to a PVDF membrane, and subsequently incubated with primary antibodies followed by HRP-conjugated secondary antibodies. Western blotting antibodies were purchased from Abcam (Cambridge, UK) and Proteintech (Rosemont, IL, USA). The resulting images were captured using the Tanon 5200 Imaging Analysis System (Shanghai,

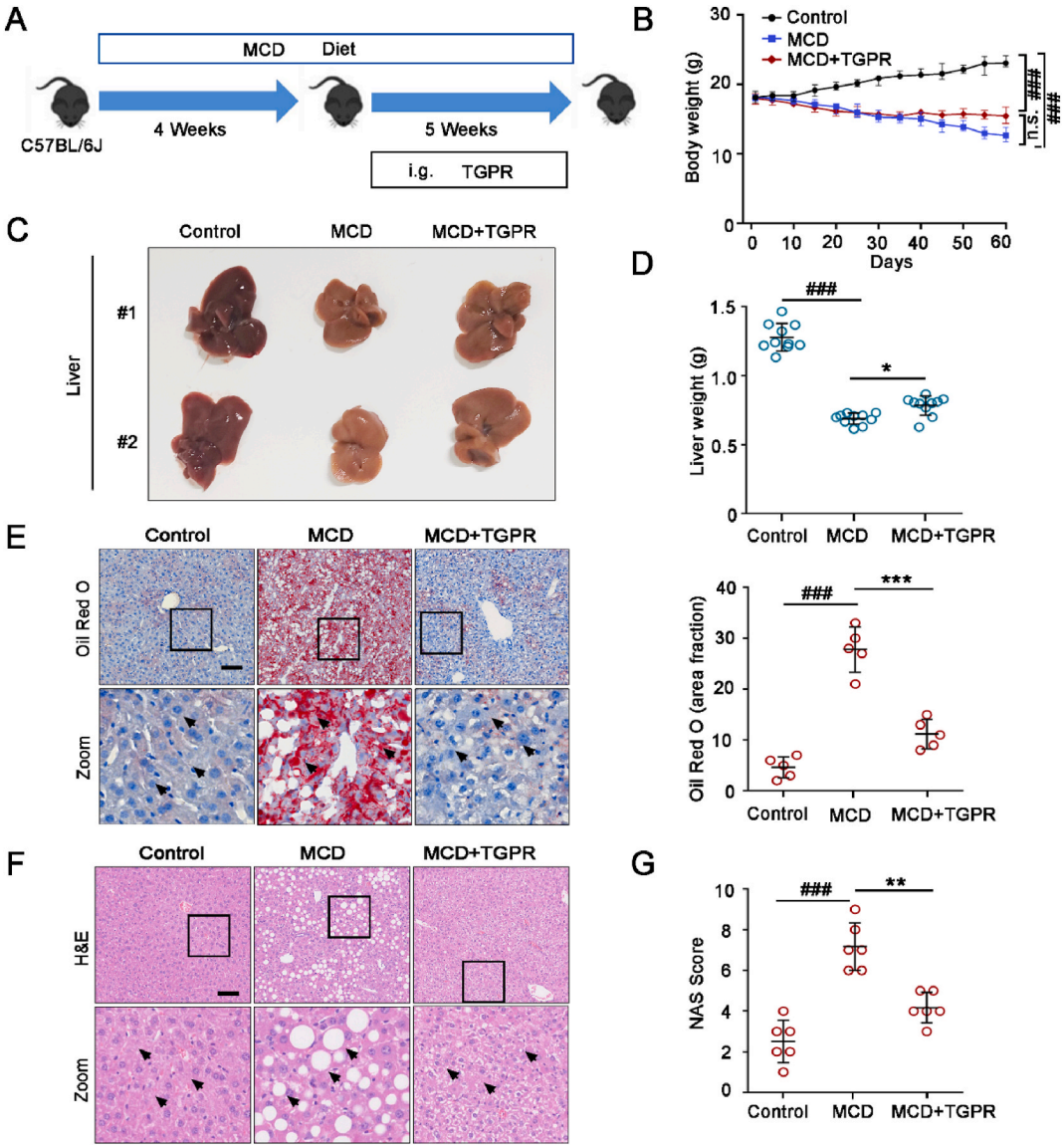

Fig. 2. TGPR alleviates MCD diet-induced NASH. (A) Schematic representation of the administration procedure of TGPR in the established MCD-feeding C57BL/6J mice. (B) Body weight changes were monitored during the experimental procedure (n = 10). (C) Representative liver images and (D) liver weights of normal and MCD mice with or without TGPR treatment. (E) Representative histology images of Oil Red O staining are shown (n = 3, scale bar = 100 μm). (F) Representative images of H&E staining of liver sections are shown (n = 3, scale bar = 100 μm). (G) NAS score was assessed in H&E-stained liver sections. NAS scoring index: steatosis (0–3), lobular inflammation (0–3) and hepatocyte ballooning (0–3). A total of six areas (3 × 3 mm each) were counted. The data are expressed as the mean ± SD, $^{###}P < 0.001$, MCD group compared with control group. $^{*}P < 0.05$, $^{**}P < 0.01$, $^{***}P < 0.001$, TGPR group compared with MCD group; n. s. not significant. (For interpretation of the references to color in this figure legend, the reader is referred to the Web version of this article.)

China). The signal intensities were quantified using ImageJ and normalized to the GAPDH signal.

3. Results

3.1. Identification of TGPR components

To identify the chemical constituents of TGPR, we performed HPLC assays to quantify the phytoconstituents. According to the

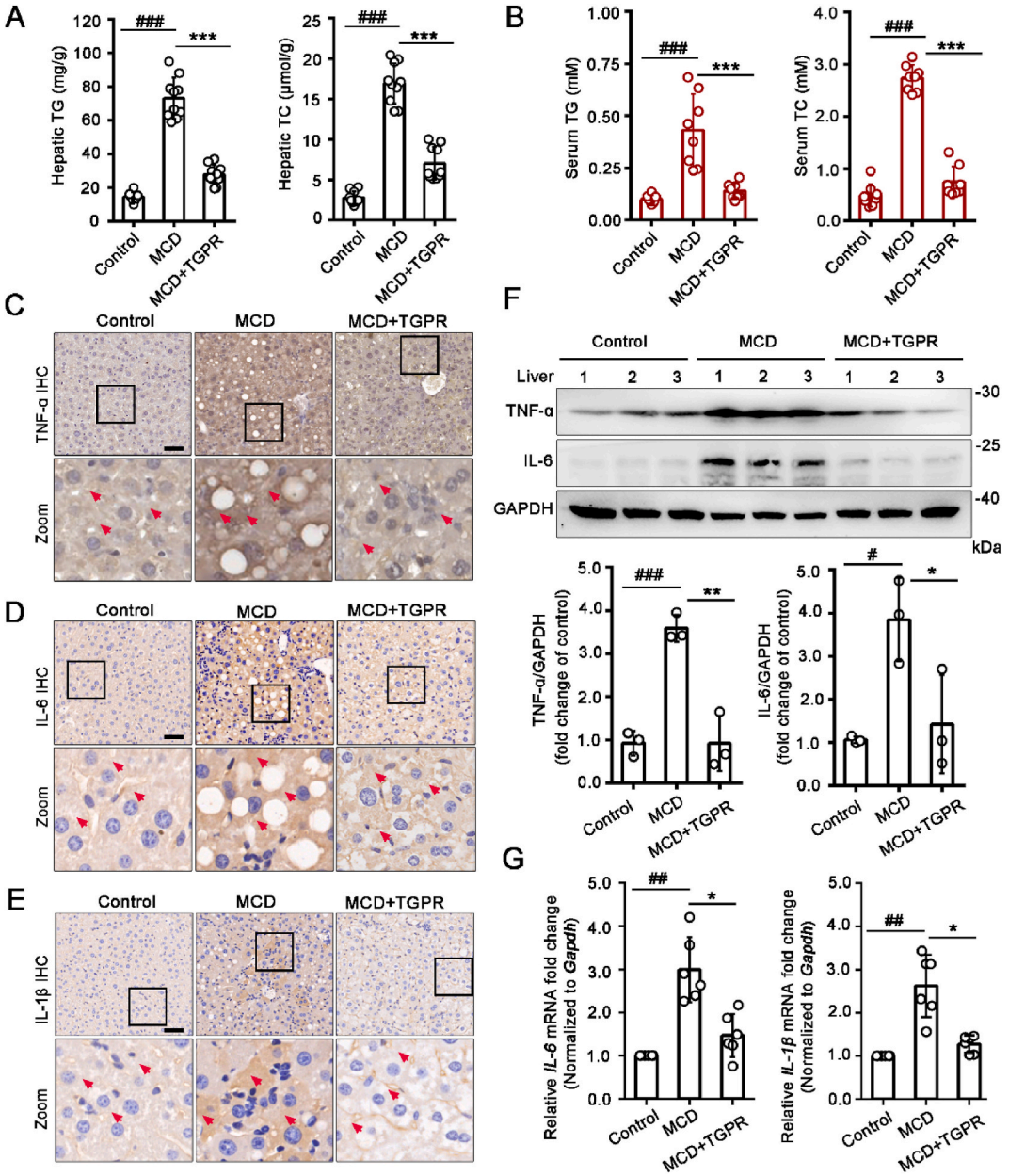

Fig. 3. TGPR effectively ameliorates hepatic dysfunction by inhibiting inflammation in MCD-fed mice. (A) Hepatic triglyceride (TG) and total cholesterol (TC) content in mice fed a normal or MCD diet, with or without TGPR treatment (n = 10). (B) Serum levels of TG and TC in mice fed a normal or MCD diet, with or without TGPR treatment (n = 8). (C) Immunohistochemistry was performed to detect the expression of TNF-α in the liver of mice (n = 3, scale bar = 100 μm). (D) Immunohistochemistry was performed to detect the expression of IL-6 in the liver of mice (n = 3, scale bar = 100 μm). (E) Immunohistochemistry was performed to detect the expression of IL-1β in the liver of mice (n = 3, scale bar = 100 μm). (F) Western blot analysis was used to detect the protein expression of TNF-α and IL-6 (mean ± SD, n = 3). (G) The expression of IL-6 and IL-1β mRNA in the liver of mice treated with TGPR was assessed by qRT-PCR (mean ± SD, n = 6). $^{\#}P < 0.5$, $^{\#\#}P < 0.01$, $^{\#\#\#}P < 0.001$, MCD group compared with control group; $^{*}P < 0.5$, $^{**}P < 0.01$, $^{***}P < 0.001$, TGPR group compared with MCD group.

standard curve and retention time of each standard compound, nine active constituents of TGPR, including Piceoside, Androsin, Vanillic acid, Picroside IV, Picroside III, Picroside II, Picroside I, 6-feruloylcatalpol, and Verminoside, were successfully identified (Fig. 1A and B). The consistent results of the HPLC chromatogram with previous reports indicate that the quality control of TGPR is deemed qualified [18].

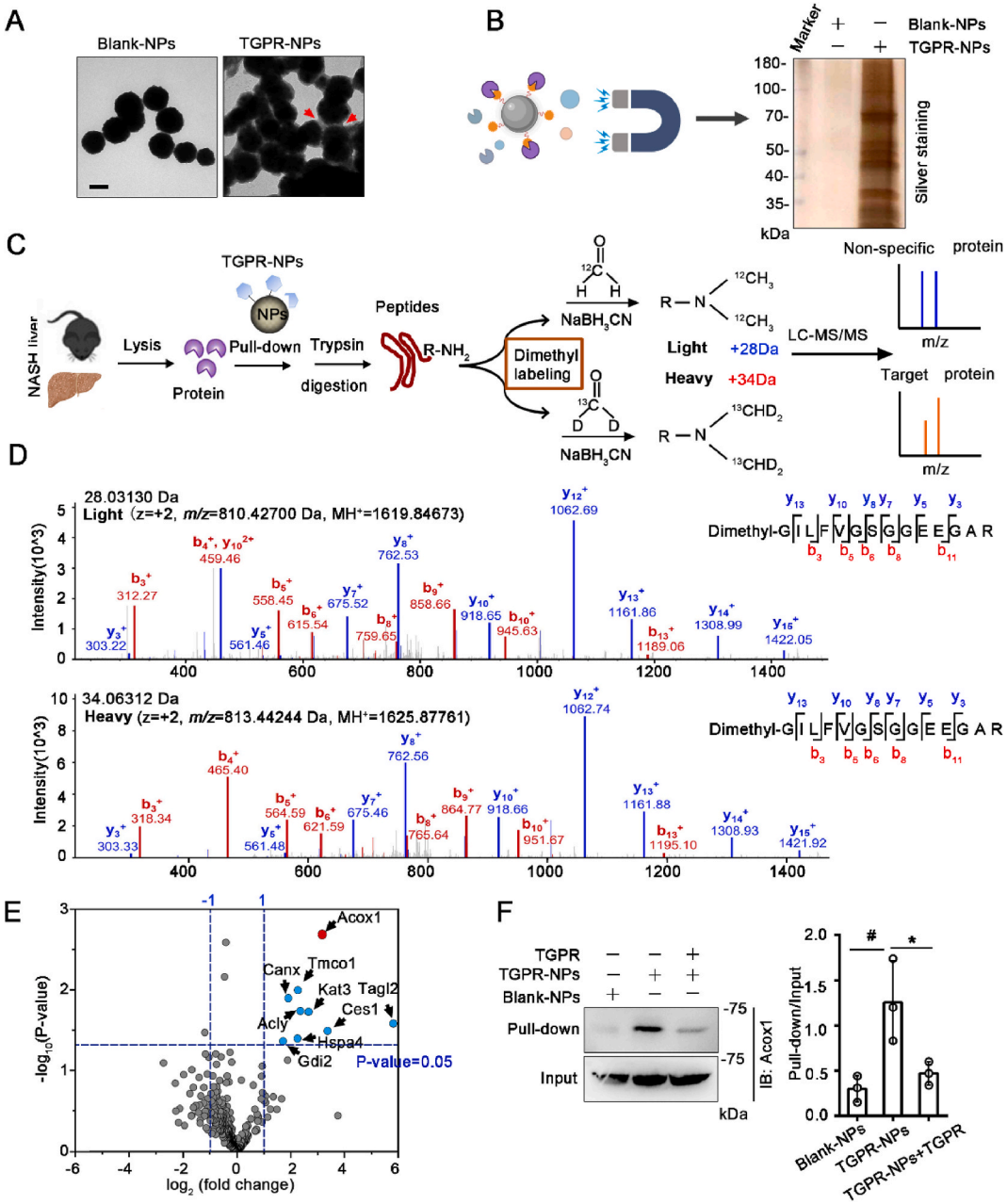

Fig. 4. Identification of the cellular targets of TGPR in the livers of NASH mice. (A) TEM image of blank-NPs and TGPR-NPs (scale bar = 100 nm). (B) Silver staining was conducted to compare NASH liver lysate with blank-NPs or TGPR–NPs. (C) The workflow for target identification of the chemical extract from TGPR was performed using pull-down and mass spectrometry. (D) Quantification was carried out using the isotopic cluster of heavy (m/z = 810.42700) and light (m/z = 813.44244) forms of the peptides. (E) A volcano plot was generated to visualize the TGPR-targeted proteins. (F) Proteins that exhibited specific binding to TGPR were identified (n = 3). $^{\#}P < 0.5$, TGPR-NPs group compared with Blank-NPs group; $^{*}P$ value < 0.5, TGPR-NPs + TGPR group compared with TGPR-NPs group.

3.2. TGPR alleviates MCD diet-induced NASH

To explore the hepatoprotective activity of TGPR in NASH, we generated the methionine-choline deficient (MCD) diet-induced NASH model in C57BL/6J mice, followed by intragastric administration with TGPR (36.2 mg/kg) from the fifth week (Fig. 2A). A successful NASH model was induced by MCD feeding over a period of 4 weeks. This model was characterized by significant reductions in body weight, liver weight, and food intake compared to mice fed a normal diet. We observed that TGPR treatment did not significantly mitigate the loss of body weight (Fig. 2B). However, it did alleviate the weight loss of the liver (Fig. 2C and D). H&E staining revealed that NASH mice displayed evident vacuolated hepatocytes and macrovesicular steatosis accompanied by pronounced inflammatory cell infiltration (Fig. 2F). Notably, these symptoms were significantly reduced by TGPR treatment, as depicted in Fig. 2F. Similarly, treatment with TGPR resulted in a reduction in hepatic lipid accumulation, as demonstrated by liver sections stained with Oil Red O (Fig. 2E). In addition, TGPR treatment led to the amelioration of liver damage, as evidenced by the NAS score being similar to that observed in the control group (Fig. 2G). Taken together, these data demonstrate that treatment with TGPR can effectively improve MCD diet-induced liver dysfunction including steatosis and hepatic ballooning.

3.3. TGPR effectively ameliorates hepatic dysfunction by inhibiting inflammation in MCD-fed mice

We next investigated the protective role of TGPR in lipid metabolism dysregulation induced by MCD. Triglyceride (TG) and total cholesterol (TC) are pivotal clinical parameters that provide valuable insights into lipid metabolism. Previous studies have consistently demonstrated that liver steatosis induced by MCD diet can result in the excessive accumulation of TG and TC within hepatocytes [21]. In line with these findings, our investigation revealed a significant increase in hepatic lipid accumulation, particularly elevated levels of TG and TC, in the MCD diet group compared to the control. Importantly, TGPR demonstrated a notable ability to reduce the excessive accumulation of both TG and TC in the liver and serum of mice with NASH (Fig. 3A and B). These results provide compelling evidence that TGPR has a remarkable capacity to alleviate hepatic dysfunction caused by the MCD diet.

Inflammation is a prominent hallmark of the pathological progression observed in NASH [22]. In MCD-induced NASH mice, injured hepatocytes secrete various pro-inflammatory cytokines, contributing to hepatic inflammation. Given the crucial role of inflammation in hepatic dysfunction associated with NASH, we assessed the anti-inflammatory effects of TGPR to mitigate this dysfunction. Indeed, MCD-induced liver inflammation in NASH mice was evident, as indicated by elevated levels of TNF-α, IL-6, and IL-1β. Immunohistochemical staining confirmed that TGPR administration significantly reduced hepatic inflammation by downregulating the expression of these inflammatory mediators compared to the MCD group (Fig. 3C–E). Moreover, this finding is corroborated by a significant decrease in TNF-α and IL-6 levels observed through immunoblotting analysis (Fig. 3F). Additionally, the mRNA expression of IL-6 and IL-1β was significantly suppressed in samples treated with TGPR (Fig. 3G). Therefore, these findings strongly indicate that TGPR exerts a potent inhibitory effect on the inflammatory response associated with hepatic dysfunction in NASH.

3.4. TGPR alleviates high-fat diet (HFD) diet-induced NASH

To investigate the potential therapeutic effect of TGPR on NASH, we also administered high-fat diet (HFD)-fed mice with oral gavage of TGPR or positive agent silybin for 4 weeks (Fig. S1A). During the 6-week treatment in HFD-fed animals, TGPR treatment improved hepatocyte injury symptoms and reduced liver lipid accumulation, as indicated by lower serum concentrations of TG and TC compared to control mice (Fig. S1B). Additionally, TGPR significantly decreased serum alanine transaminase (ALT) and aspartate aminotransferase (AST) levels, (Fig. S1C), indicating that TGPR treatment promotes effective liver protection in NASH. Furthermore, ELISA assays revealed that TGPR alleviated elevated IL-6 and TNF-α levels in an HFD-induced NASH model (Fig. S1D), demonstrating the effectiveness of TGPR in reducing inflammation. Collectively, these data suggest that TGPR effectively improves NASH symptoms in MCD and HFD-induced models.

3.5. Identification of the cellular targets of TGPR in the livers of NASH mice

To explore the underlying mechanisms whereby TGPR suppresses NASH progression, we identified the specific target proteins that bind to TGPR in the livers of mice. We first employed TGPR-crosslinked nanoparticles (TGPR-NPs), which were designed to capture the potential target proteins. As depicted in Fig. 4A, TEM analysis revealed that TGPR-NPs had a characteristic core (Fe_3O_4)-shell (TGPR) structure, indicating successful crosslinking of TGPR onto the NPs. Subsequently, a pull-down assay, based on the principle of affinity purification, was conducted using TGPR-NPs to efficiently capture and identify the specific proteins present in the liver lysate of mice with NASH. The NPs-captured proteins were then visualized through silver staining (Fig. 4B). Next, the proteins bound to the NPs were eluted and digested into peptides using trypsin. Isotopic labeling was performed on the N-terminal of the peptide and the ε-amino group of lysine using a combination of isotopic isomers of formaldehyde and cyanoborohydride. The labeled samples were mixed together and subjected to simultaneous analysis using LC-MS.

To execute the dimethyl labeling MS analysis strategy, we utilized formaldehyde/$NaCNBH_3$ or deuterated formaldehyde/$NaCNBD_3$ treatments. These treatments induced a mass difference of 6 Da between the peptides derived from the two distinct groups (Fig. 4C and D). Then, we successfully identified 553 proteins, as depicted in the volcano scatter plot (Fig. 4E). After analyzing the mass spectrometric data, we conducted a screening process to identify potential targets for the anti-NASH effects of TGPR. As a result, we shortlisted 9 candidates: Tagl2, Ces1, Acox1, Kat3, Acly, Tmco1, Hspa4, Canx, and Gdi2, which make them potential targets for further investigation. Notably, previous studies have demonstrated the significance of Acox1, an enzyme responsible for fatty acid oxidation.

Acox1 plays a vital role in the regulation of very long-chain fatty acids, leading to increased energy expenditure in the liver [23,24]. Therefore, we hypothesized that Acox1 could be a crucial cellular target of TGPR to treat NASH. To further validate the direct interaction between TGPR and Acox1, we conducted a pull-down analysis. Immunoblotting using an Acox1 antibody was then performed to confirm the direct interaction of TGPR with Acox1 (Fig. 4F). Taken together, these results suggest that Acox1 is a key cellular target of TGPR for anti-NASH.

3.6. *Major components in TGPR bind to Acox1 revealed by docking analysis*

A recent study revealed that the six bioactive constituents of TGPR were identified in the liver following oral administration, including Picroside I, Picroside II, Picroside IV, Vanillic acid, Androsin, and Cinnamic acid [18]. Notably, most of these metabolites, such as Picroside I, Picroside II, and Picroside IV, demonstrated significant hepatoprotective effects [18]. To determine the binding pattern of TGPR to Acox1, we performed molecular docking experiments with the major components of TGPR (such as Picroside I, Picroside II, and Picroside IV) and the Acox1 protein. The findings indicate that the compound Picroside I binds preferentially to residues 102–423 within the C-domain of the target protein Acox1, forming hydrogen bond interactions with Y136, Q138, T139, G144,

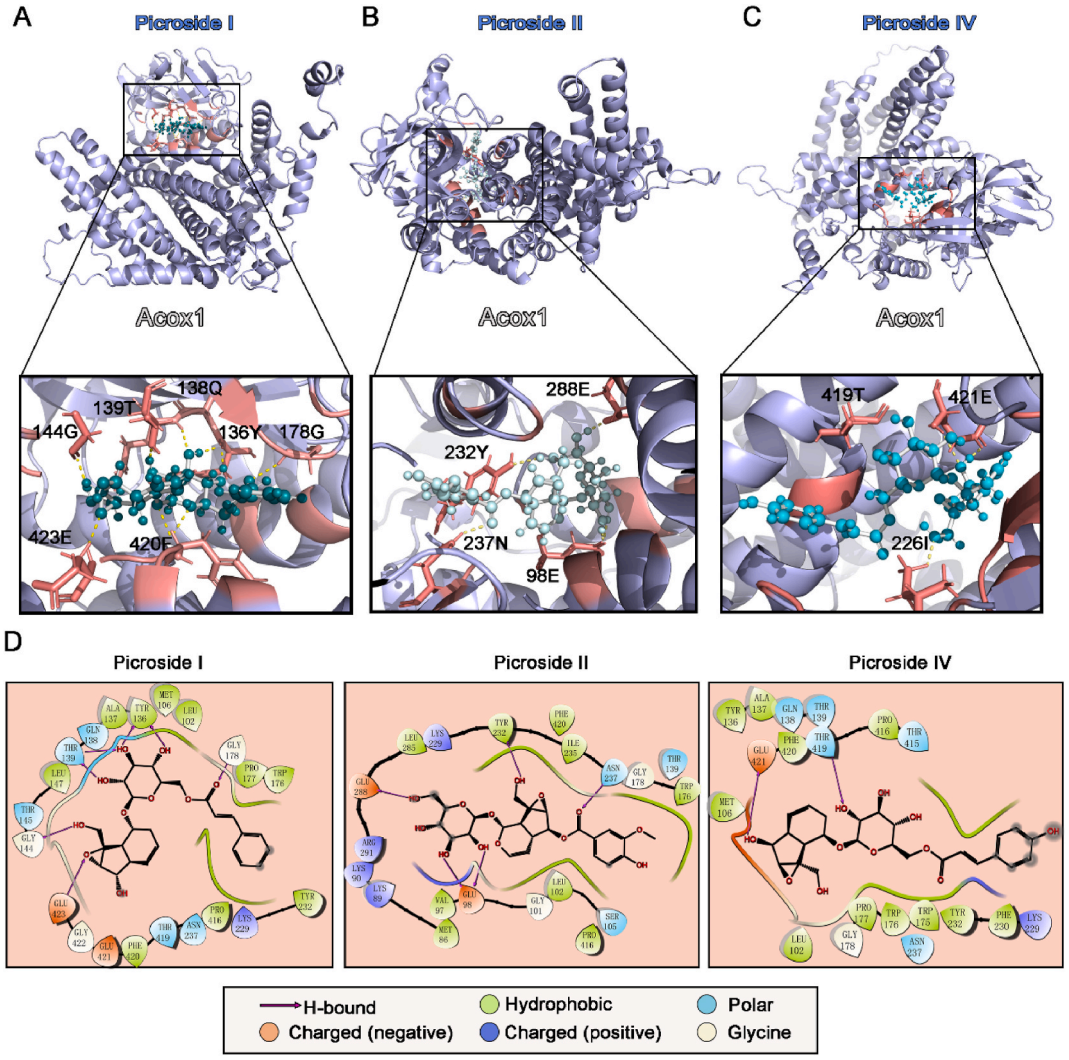

Fig. 5. Major components in TGPR bind to Acox1 revealed by docking analysis. (A) Docking model of Picroside I into the structure of Acox1 (AlphaFold: AF-Q9R0H0-F1). The homology model of Acox1 is shown in purple ribbon and surface, with hydrogen bonds depicted as yellow dashed lines (136Y, 139T, 144G, 178G, 420F, and 423E). (B) Docking model of Picroside II into the structure of Acox1 (AlphaFold: AF-Q9R0H0-F1). The homology model of Acox1 is shown in purple ribbon and surface, with hydrogen bonds depicted as yellow dashed lines (98E, 232Y, 237N and 288E). (C) Docking model of Picroside IV into the structure of Acox1 (AlphaFold: AF-Q9R0H0-F1). The homology model of Acox1 is shown in purple ribbon and surface, with hydrogen bonds depicted as yellow dashed lines (226I and 421E). (D) 2D representation depicting the frequencies of protein-molecular interactions. (For interpretation of the references to color in this figure legend, the reader is referred to the Web version of this article.)

F420, and E423 (Fig. 5A). Picroside II exhibits significant binding ability to Acox1, primarily achieved through the formation of intermolecular hydrogen bonds involving residues E98, Y232, N237, and E288 (Fig. 5B). Additionally, Picroside IV binds to the motif (residues 102–421) in the Acox1 protein by forming two hydrogen bonds with residues I226 and E421 (Fig. 5C). Taken together, these results suggest that the major components of TGPR, such as Picroside I, Picroside II, and Picroside IV, have significant binding ability to the target protein Acox1.

Acox1 is comprised of an N-terminal α-domain (residues 1–130), a middle β-domain (residues 131–270), and a catalytic C-terminal α-domain (residues 271–654) [24]. It is reported that Acox1 possesses a large active site located near the C-terminal α-domain, enabling it to accommodate longer ascaroside-CoA and fatty acyl-CoA substrates [25,26]. Our docking results reported that the major components of TGPR, such as Picroside I, Picroside II, and Picroside IV, preferentially bind to the C-terminal α-domain (residues approximately 102–423) of the Acox1 protein, forming hydrogen bond interactions (Fig. 5D). These data demonstrate that TGPR can bind to the catalytic region of the Acox1 protein following liver metabolism, thereby regulating downstream molecular signaling pathways to exert an anti-NASH effect.

3.7. TGPR exerts its anti-NASH effect by stabilizing Acox1 protein and regulating MAPK pathways

To further assess the function of TGPR in NASH by targeting Acox1, we examined the correlation between lipid droplet abundance

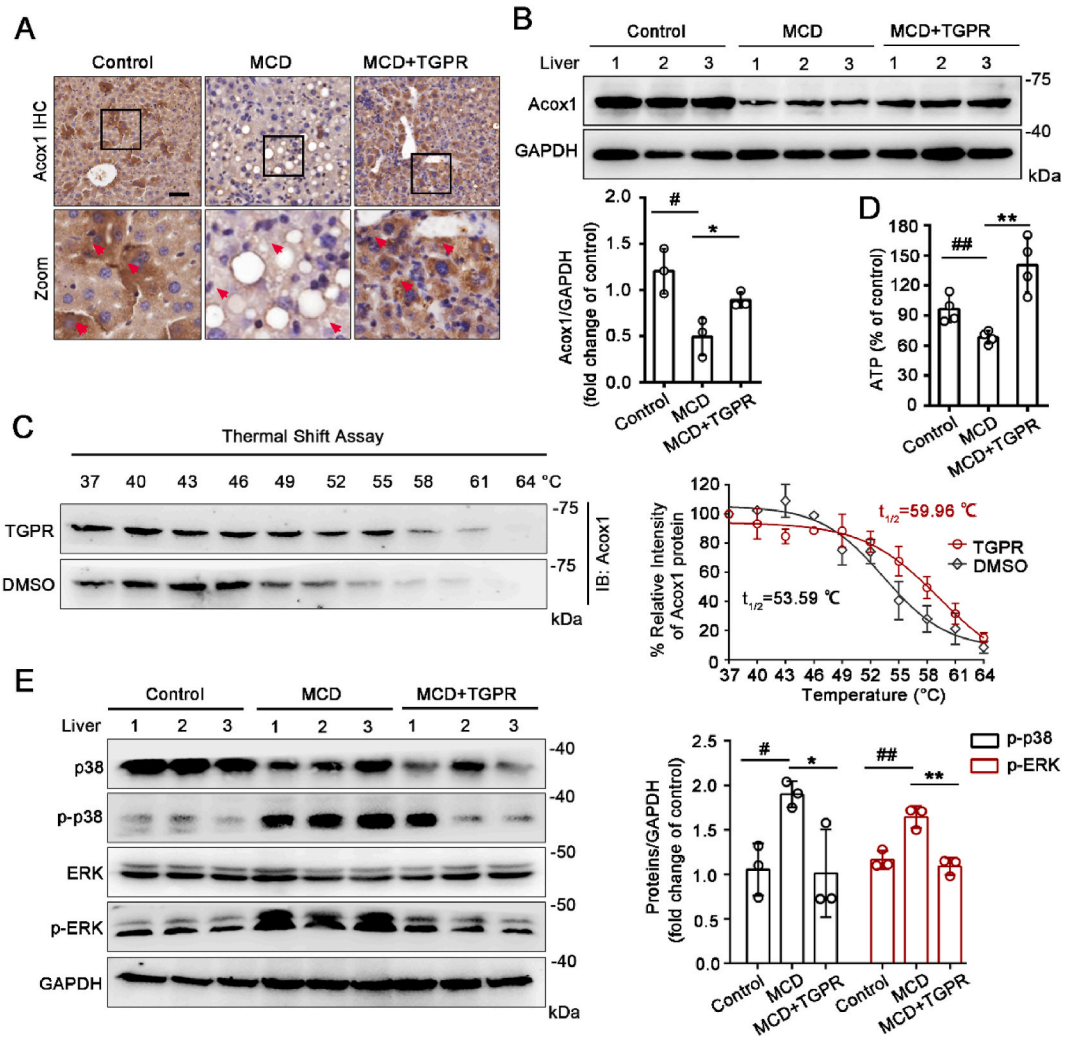

Fig. 6. TGPR exerts its anti-NASH effect by stabilizing Acox1 protein and regulating MAPK pathways. (A) Immunohistochemistry was performed to detect the expression of Acox1 in the liver of mice (n = 3, scale bar = 100 μm). (B) Expression of Acox1 in the liver of mice fed with MCD in the presence or absence of TGPR was analyzed by immunoblotting (mean ± SD, n = 3). (C) The effect of TGPR on the stability of Acox1 under different temperature gradients was evaluated using CETSA (mean ± SD, n = 3). (D) TGPR reversed the reduction in ATP levels induced by MCD feeding (mean ± SD, n = 4). (E) The protein expression of total p38, p-p38, ERK, p-ERK in MCD and TGPR-treated mice tissues (mean ± SD, n = 3). $^{\#}P < 0.5$, $^{\#\#}P < 0.01$, MCD group compared with control group; $^{*}P < 0.5$, $^{**}P < 0.01$, TGPR group compared with MCD group.

and Acox1 expression in NASH liver tissues. The expression of Acox1 protein was decreased in the liver tissues of MCD mice in comparison to the control samples. Conversely, the levels of lipid droplets were higher in the MCD-treated mice. However, this trend was reversed when the mice were treated with TGPR (Fig. 6A). Remarkably, our data revealed a significant increase in Acox1 protein level with TGPR treatment in comparison to the MCD-diet group (Fig. 6B). Based on these findings, we postulated that TGPR might enhance lipid degradation by augmenting Acox1 levels. Furthermore, we employed cellular thermal shift assays (CETSA) to determine whether TGPR could enhance the thermal stability of the Acox1 protein. Our findings indicated that TGPR significantly affected the thermal stability of Acox1 in NASH liver lysate (Fig. 6C), suggesting that TGPR directly binds to Acox1 and enhances its stability. Therefore, our findings indicate that TGPR alleviated hepatic lipid accumulation by potentially stabilizing Acox1 protein.

Given the crucial role of Acox1 in governing hepatic energy metabolism, particularly its influence on ATP concentration, our subsequent investigation was primarily focused on evaluating ATP levels. An observed reduction in hepatic ATP content in mice fed with MCD diet suggests an aberration in fatty acid metabolism. The administration of TGPR resulted in a higher ATP concentration when compared to the MCD group, implying that TGPR possesses the capability to modulate energy metabolism pathways and influence ATP production (Fig. 6D). The MAPK signaling pathway has been shown to play an essential role in inflammatory responses and ATP production during NASH progression [27,28]. Thus, we investigated how TGPR regulates the MAPK signaling pathway to alleviate NASH pathogenesis. Our results showed that the MCD diet-induced NASH led to rapid phosphorylation of p38 and ERK in the liver, which was inhibited by TGPR treatment during the progression of NASH (Fig. 6E). Together, our findings provide evidence that TGPR plays a significant role in ameliorating NASH by stabilizing Acox1 protein and modulating the MAPK signaling pathway.

4. Discussion

Multiple studies have emphasized the crucial role of traditional herbal medicine in managing complex conditions, including NASH [29–32]. In this study, we validated the effectiveness of TGPR, a component derived from the traditional herbal medicine *Picrorhiza scrophulariiflora* Pennell, in suppressing the advancement of NASH. TGPR effectively reduced lipid levels in NASH mice, resulting in notable improvements in hepatic and serum levels of triglycerides (TG) and total cholesterol (TC). In addition, TGPR demonstrated a substantial inhibitory impact on lipid accumulation, leading to an effective decrease in the aggregation of inflammatory cells and the formation of fibrosis. These findings significantly enhance our understanding of the therapeutic role of TGPR in NASH and provide evidence to support its rational use in future clinical considerations.

The identification of drug targets plays a crucial role in understanding how drugs exert their therapeutic effects [33,34]. To explore the molecular target responsible for alleviating NASH with TGPR, we utilized a "target fishing" strategy based on the principle of affinity purification, developed in our laboratory, to synthesize TGPR-crosslinked nanoparticles (NPs) [19]. The surface-immobilized TGPR of nanoparticles enable the direct capture and enrichment of target proteins from liver tissue lysates (target protein library) based on the principle of ligand-target specific recognition. Meanwhile, we employed dimethyl labeling strategy to perform quantitative proteomics analysis on the captured target proteins [17,35]. The application of these techniques in combination facilitated the successful identification of the protein target spectrum directly associated with the intricate TGPR complex system, thereby facilitating subsequent investigations into its molecular mechanisms. Notably, we identified a total of 9 major target proteins of TGPR, including Tagl2, Ces1, Acox1, Kat3, Acly, Tmco1, Hspa4, Canx, and Gdi2. We have shown that Acox1 is pivotal in the anti-NASH effects of TGPR. Moreover, other constituents of TGPR may interact with diverse molecular targets, thereby contributing to its therapeutic efficacy against NASH. For example, Acly plays a critical role in lipid synthesis [36,37], while Hspa4 is implicated in cellular stress responses linked to NASH pathogenesis [38]. Of note, identifying synergistic interactions among these targets underscores the importance of conducting comprehensive research in future investigations.

Acox1 plays a critical role in NASH progression and may offer a potential target for therapeutic intervention. For example, Saikosaponin D, derived from *Radix Bupleuri*, has been reported to induce Acox1 expression in the liver, facilitating fatty acid degradation and suppressing NAFLD development [39]. Similarly, pharmacological treatment of diet-induced NASH mice with Schisandrin B restored Acox1 expression, reduced inflammation-induced hepatocyte injury, and improved lipid metabolism [40]. Additionally, NASH-hepatic tissues from HFHC diet-fed mice exhibited significantly reduced Acox1 levels, and this reduction was mitigated by supplementation with Gentiopicroside, a traditional medicine with anti-inflammatory properties [41]. Consistent with these studies, we found that TGPR, the primary active ingredient of *Picrorhiza scrophulariiflora* Pennell, effectively countered the decrease in Acox1 protein levels by binding predominantly to the catalytic C-terminal α-domain, thereby stabilizing the Acox1 protein, regulating lipid metabolism, and suppressing NASH pathogenesis.

Accumulating evidence has shown that Acox1 plays a crucial role in maintaining hepatic lipid balance and modulating NASH progression [42–44]. However, regardless of whether Acox1 acts as an activator or suppressor of NASH, its regulation of NASH development is contingent upon its enzymatic catalytic function. Peroxisomal Acox1, a key enzyme in fatty acid β-oxidation, has been widely studied for its pivotal role in fatty acid metabolism [45]. Preliminary studies indicate a stronger association between macrophage activation and very long-chain fatty acids as well as β-oxidation [46,47]. Of note, hepatocytes and macrophages exhibit distinct responses and effects on β-oxidation. In addition to hepatocytes, activated macrophages also utilize β-oxidation of fatty acids and oxidative phosphorylation to produce energy-rich molecules such as ATP, playing a role in tissue repair and the inhibition of inflammation [48]. Thus, we assume that macrophages are likely the primary target cells of TGPR. This hypothesis was based on the following phenomenon: (1) TGPR exhibit significant immunomodulatory effects [49,50]. Previous studies have demonstrated the essential role of Picroside II in the activation of M1-polarized macrophages [51]. Given this knowledge, we hypothesized that TGPR may regulate NASH by modulating macrophages activation. (2) Abundant studies have reported the hepatic lipid-laden foamy macrophages have been associated with the severity of steatosis and steatohepatitis in NAFLD patients [52,53]. Combined with our

findings that TGPR positively affects Acox1 expression and lipid droplet metabolism in MCD-induced NASH, we assumed that TGPR may influence macrophage activity related to lipid droplets. But how TGPR induces macrophage activation is still not well understood and needs further investigation.

Due to the significant involvement of Acox1-mediated lipid metabolism in liver function, the primary aim of our research is to investigate the potential impact of TGPR binding to Acox1 and its subsequent influence on signaling pathways. Our results demonstrate that TGPR exhibits binding affinity towards Acox1, as confirmed by pull-down and CETSA analysis. Notably, we found that TGPR has a positive impact on the regulation of Acox1 expression and lipid droplets metabolism in mice. Based on these observations, the docking results indicated that the major components of TGPR, including Picroside I, Picroside II, and Picroside IV, show a preference for binding to the C-terminal α-domain of the Acox1 protein, specifically around residues 86–423. Our hypothesis suggests that following liver metabolism, TGPR can directly interact with Acox1, potentially enhancing protein stability through induced conformational changes and simultaneously regulating enzyme activity. Although further analysis is required, our current findings provide a new perspective on the potential therapeutic applications of natural products in the regulation of Acox1 for the treatment of NASH.

5. Conclusion

In summary, our study offers valuable insights into the potential therapeutic benefits of TGPR in alleviating the pathological progression of NASH. Specifically, our findings reveal that TGPR exerts its beneficial effects by selectively modulating the Acox1-mediated signaling pathway in hepatic cells. Hence, our study highlights the promising therapeutic potential of TGPR as a novel and efficacious treatment approach for NASH.

CRediT authorship contribution statement

Fang-Fang Zhuo: Writing – original draft, Data curation. **Xiao-Qing Li:** Investigation, Data curation. **Jun Zhang:** Methodology, Data curation. **Fu-Ming Zhang:** Software, Investigation. **Zhao-Hui Song:** Validation, Software. **Yi He:** Validation. **Li Ding:** Methodology, Data curation. **Dan Liu:** Data curation. **Peng-Fei Tu:** Project administration, Investigation. **Xiao-Hui Ma:** Project administration, Data curation. **Ke-Wu Zeng:** Writing – review & editing.

Availability of data and materials

Data for the review paper are all included to the document and hence no other data available.

Declaration of competing interest

The authors declare that they have no known competing financial interests or personal relationships that could have appeared to influence the work reported in this paper.

Acknowledgements

This work was financially supported by National Natural Sciences Foundation of China (82325050), Beijing Municipal Natural Science Foundation (7232273), Jinan New 20 Policies for Higher Education Funding (202228048), Natural Science Foundation of Shandong Province (Joint Fundation for Innovation and Development) (ZR2022LZY021), the Special Fund for “Tian-Chi Talent Introduction Program”, and the Special Fund for Taishan Scholars Project in Shandong Province (tstp20230633).

Appendix A. Supplementary data

Supplementary data to this article can be found online at https://doi.org/10.1016/j.heliyon.2024.e39874.

References

[1] R. Loomba, A. Sanyal, The global NAFLD epidemic, Nat. Rev. Gastroenterol. Hepatol. 10 (2013) 686–690, https://doi.org/10.1038/nrgastro.2013.171.
[2] X. Xu, K.L. Poulsen, L. Wu, S. Liu, T. Miyata, Q. Song, et al., Targeted therapeutics and novel signaling pathways in non-alcohol-associated fatty liver/steatohepatitis (NAFL/NASH), Signal Transduct. Targeted Ther. 7 (1) (2022) 287, https://doi.org/10.1038/s41392-022-01119-3.
[3] S. Schuster, D. Cabrera, M. Arrese, A.E. Feldstein, Triggering and resolution of inflammation in NASH, Nat. Rev. Gastroenterol. Hepatol. 15 (6) (2018) 349–364, https://doi.org/10.1038/s41575-018-0009-6.
[4] S.A. Harrison, A.M. Allen, J. Dubourg, M. Noureddin, N. Alkhouri, Challenges and opportunities in NASH drug development, Nat. Med. 29 (3) (2023) 562–573, https://doi.org/10.1038/s41575-018-0009-6.
[5] T. Hashimoto, Peroxisomal beta-oxidation: enzymology and molecular biology, Ann. N. Y. Acad. Sci. 804 (1996) 86–98, https://doi.org/10.1111/j.1749-6632.1996.tb18610.x.
[6] A.J. Stauber, H. Brown-Borg, J. Liu, M.P. Waalkes, A. Laughter, R.A. Staben, et al., Constitutive expression of peroxisome proliferator-activated receptor alpha-regulated genes in dwarf mice, Mol. Pharmacol. 67 (3) (2005) 681–694, https://doi.org/10.1111/j.1749-6632.1996.tb18610.x.

[7] H.I. El Hajj, A. Vluggens, P. Andreoletti, K. Ragot, S. Mandard, S. Kersten, et al., The inflammatory response in acyl-CoA oxidase 1 deficiency (pseudoneonatal adrenoleukodystrophy), Endocrinology 153 (6) (2012) 2568–2575, https://doi.org/10.1210/en.2012-1137.

[8] J. Huang, N. Viswakarma, S. Yu, Y. Jia, L. Bai, A. Vluggens, et al., Progressive endoplasmic reticulum stress contributes to hepatocarcinogenesis in fatty acyl-CoA oxidase 1-deficient mice, Am. J. Pathol. 179 (2) (2011) 703–713, https://doi.org/10.1016/j.ajpath.2011.04.030.

[9] X.F. Chen, M.X. Tian, R.Q. Sun, M.L. Zhang, L.S. Zhou, L. Jin, et al., SIRT5 inhibits peroxisomal ACOX1 to prevent oxidative damage and is downregulated in liver cancer, EMBO Rep. 19 (5) (2018) e45124, https://doi.org/10.15252/embr.201745124.

[10] J.J. Wang, Y.T. Zhang, Y.J. Tseng, J. Zhang, miR-222 targets ACOX1, promotes triglyceride accumulation in hepatocytes, Hepatobiliary Pancreatic Dis. Int. 18 (4) (2019) 360–365, https://doi.org/10.1016/j.hbpd.2019.05.002.

[11] M.B. Rokaya, B. Parajuli, K.P. Bhatta, B. Timsina, Neopicrorhiza scrophulariiflora (Pennell) Hong: a comprehensive review of its traditional uses, phytochemistry, pharmacology and safety, J. Ethnopharmacol. 247 (2020) 112250, https://doi.org/10.1016/j.jep.2019.112250.

[12] D. Kumar, R. Kumar, B. Singh, P.S. Ahuja, Comprehensive chemical profiling of Picrorhiza kurroa royle ex benth using NMR, HPTLC and LC-MS/MS techniques, Comb. Chem. High Throughput Screening 19 (3) (2016) 200–215, https://doi.org/10.2174/1386207319666160114092538.

[13] X. Xu, W.T. Wang, Z.Y. Zhao, W.G. Xi, B. Yu, C.H. Hao, et al., Effects of total iridoid glycosides of Picrorhiza scrophulariiflora against non-alcoholic steatohepatitis rats induced by high-fat and high-sugar diet through regulation of lipid metabolism, Chin. Herb Med. 12 (1) (2020) 67–72, https://doi.org/10.1016/j.chmed.2019.12.005.

[14] K. Xiong, M. Shi, T. Zhang, H. Han, Protective effect of picroside I against hepatic fibrosis in mice via sphingolipid metabolism, bile acid biosynthesis, and PPAR signaling pathway, Biomed. Pharmacother. 131 (2020) 110683, https://doi.org/10.1016/j.biopha.2020.110683.

[15] N. Zhou, Y. Zhu, M. Hu, R. Zheng, M. Sun, Y. Bian, et al., Evaluation potential effects of Picroside II on cytochrome P450 enzymes in vitro and in vivo, J. Ethnopharmacol. 314 (2023) 116582, https://doi.org/10.1016/j.jep.2023.116582.

[16] J.L. Hsu, S.Y. Huang, N.H. Chow, S.H. Chen, Stable-isotope dimethyl labeling for quantitative proteomics, Anal. Chem. 75 (24) (2003) 6843–6852, https://doi.org/10.1021/ac0348625.

[17] P.J. Boersema, R. Raijmakers, S. Lemeer, S. Mohammed, A.J. Heck, Multiplex peptide stable isotope dimethyl labeling for quantitative proteomics, Nat. Protoc. 4 (4) (2009) 484–494, https://doi.org/10.1038/nprot.2009.21.

[18] J. Wu, Z. Song, N. Cai, N. Cao, Q. Wang, X. Xiao, et al., Pharmacokinetics, tissue distribution and excretion of six bioactive components from total glucosides picrorhizae rhizoma, as simultaneous determined by a UHPLC-MS/MS method, J. Chromatogr., B: Anal. Technol. Biomed. Life Sci. 1227 (2023) 123830, https://doi.org/10.1016/j.jchromb.2023.123830.

[19] M.M. Zhao, L. Yao, X.W. Zhang, L.C. Wang, P.F. Tu, K.W. Zeng, Global identification of the cellular targets for a multi-molecule system by a photochemically-induced coupling reaction, Chem. Commun. 57 (28) (2021) 3449–3452, https://doi.org/10.1039/d1cc00392e.

[20] F.F. Zhuo, L. Li, T.T. Liu, X.M. Liang, Z. Yang, Y.Z. Zheng, et al., Lycorine promotes IDH1 acetylation to induce mitochondrial dynamics imbalance in colorectal cancer cells, Cancer Lett. 573 (2023) 216364, https://doi.org/10.1016/j.canlet.2023.216364.

[21] Q.M. Anstee, G. Targher, C.P. Day, Progression of NAFLD to diabetes mellitus, cardiovascular disease or cirrhosis, Nat. Rev. Gastroenterol. Hepatol. 10 (6) (2013) 330–344, https://doi.org/10.1038/nrgastro.2013.41.

[22] A.C. Sheka, O. Adeyi, J. Thompson, B. Hameed, P.A. Crawford, S. Ikramuddin, Nonalcoholic steatohepatitis: a review, JAMA, J. Am. Med. Assoc. 323 (12) (2020) 1175–1183, https://doi.org/10.1001/jama.2020.2298.

[23] M.E. Moreno-Fernandez, D.A. Giles, T.E. Stankiewicz, R. Sheridan, R. Karns, M. Cappelletti, et al., Peroxisomal β-oxidation regulates whole body metabolism, inflammatory vigor, and pathogenesis of nonalcoholic fatty liver disease, JCI Insight 3 (6) (2018) e93626, https://doi.org/10.1172/jci.insight.93626.

[24] R.R. Sonani, A. Blat, G. Dubin, Crystal structures of apo- and FAD-bound human peroxisomal acyl-CoA oxidase provide mechanistic basis explaining clinical observations, Int. J. Biol. Macromol. 205 (2022) 203–210, https://doi.org/10.1016/j.ijbiomac.2022.02.008.

[25] X. Zhang, K. Li, R.A. Jones, S.D. Bruner, R.A. Butcher, Structural characterization of acyl-CoA oxidases reveals a direct link between pheromone biosynthesis and metabolic state in Caenorhabditis elegans, Proc. Natl. Acad. Sci. U. S. A 113 (36) (2016) 10055–10060, https://doi.org/10.1073/pnas.1608262113.

[26] X. Zhang, Y. Wang, D.H. Perez, R.A. Jones Lipinski, R.A. Butcher, Acyl-CoA oxidases fine-tune the production of ascaroside pheromones with specific side chain lengths, ACS Chem. Biol. 13 (4) (2018) 1048–1056, https://doi.org/10.1021/acschembio.7b01021.

[27] E.E. Vargas-Pozada, E. Ramos-Tovar, J.D. Rodriguez-Callejas, I. Cardoso-Lezama, S. Galindo-Gómez, D. Talamás-Lara, et al., Caffeine inhibits NLRP3 inflammasome activation by downregulating TLR4/MAPK/NF-κB signaling pathway in an experimental NASH model, Int. J. Mol. Sci. 23 (17) (2022) 9954, https://doi.org/10.3390/ijms23179954.

[28] Z.M. Younossi, A. Karrar, M. Pierobon, A. Birerdinc, M. Stepanova, D. Abdelatif, et al., An exploratory study examining how nano-liquid chromatography-mass spectrometry and phosphoproteomics can differentiate patients with advanced fibrosis and higher percentage collagen in non-alcoholic fatty liver disease, BMC Med. 16 (1) (2018) 170, https://doi.org/10.1186/s12916-018-1136-1.

[29] L. Xue, K. Liu, C. Yan, J. Dun, Y. Xu, L. Wu, et al., Schisandra lignans ameliorate nonalcoholic steatohepatitis by regulating aberrant metabolism of phosphatidylethanolamines, Acta Pharm. Sin. B 13 (8) (2023) 3545–3560, https://doi.org/10.1016/j.apsb.2023.04.009.

[30] J.M. Yang, Y. Sun, M. Wang, X.L. Zhang, S.J. Zhang, Y.S. Gao, et al., Regulatory effect of a Chinese herbal medicine formula on non-alcoholic fatty liver disease, World J. Gastroenterol. 25 (34) (2019) 5105–5119, https://doi.org/10.3748/wjg.v25.i34.5105.

[31] F. Zhou, M. Ding, Y. Gu, G. Fan, C. Liu, Y. Li, et al., Aurantio-obtusin attenuates non-alcoholic fatty liver disease through Ampk-mediated autophagy and fatty acid oxidation pathways, Front. Pharmacol. 12 (2022) 826628, https://doi.org/10.3389/fphar.2021.826628.

[32] T. Yan, N. Yan, P. Wang, Y. Xia, H. Hao, G. Wang, et al., Herbal drug discovery for the treatment of nonalcoholic fatty liver disease, Acta Pharm. Sin. B 10 (1) (2020) 3–18, https://doi.org/10.1016/j.apsb.2019.11.017.

[33] M. Schenone, V. Dančík, B.K. Wagner, P.A. Clemons, Target identification and mechanism of action in chemical biology and drug discovery, Nat. Chem. Biol. 9 (4) (2013) 232–240, https://doi.org/10.1038/nchembio.1199.

[34] C. Zhong, C. Jiang, S. Ni, Q. Wang, L. Cheng, H. Wang, et al., Identification of bioactive anti-angiogenic components targeting tumor endothelial cells in Shenmai injection using multidimensional pharmacokinetics, Acta Pharm. Sin. B 10 (9) (2020) 1694–1708, https://doi.org/10.1016/j.apsb.2019.12.011.

[35] F. Yang, J. Gao, J. Che, G. Jia, C. Wang, A dimethyl-labeling-based strategy for site-specifically quantitative chemical proteomics, Anal. Chem. 90 (15) (2018) 9576–9582, https://doi.org/10.1021/acs.analchem.8b02426.

[36] X. Feng, L. Zhang, S. Xu, A.Z. Shen, ATP-citrate lyase (ACLY) in lipid metabolism and atherosclerosis: an updated review, Prog. Lipid Res. 77 (2020) 101006, https://doi.org/10.1016/j.plipres.2019.101006.

[37] M.R. Morrow, B. Batchuluun, J. Wu, E. Ahmadi, J.M. Leroux, P. Mohammadi-Shemirani, et al., Inhibition of ATP-citrate lyase improves NASH, liver fibrosis, and dyslipidemia, Cell Metabol. 34 (6) (2022) 919–936, https://doi.org/10.1016/j.cmet.2022.05.004.

[38] L.S. Almeida, C.J. Teixeira, C.V. Campos, L.G. Casaloti, F.S. Sodré, V.C. Capetini, et al., Low birth weight intensifies changes in markers of hepatocarcinogenesis induced by fructose consumption in rats, Metabolites 12 (10) (2022) 886, https://doi.org/10.3390/metabo12100886.

[39] X. Li, J. Ge, Y. Li, Y. Cai, Q. Zheng, N. Huang, et al., Integrative lipidomic and transcriptomic study unravels the therapeutic effects of saikosaponins A and D on non-alcoholic fatty liver disease, Acta Pharm. Sin. B 11 (11) (2021) 3527–3541, https://doi.org/10.1016/j.apsb.2021.03.018.

[40] L.S. Yan, S.F. Zhang, G. Luo, B.C. Cheng, C. Zhang, Y.W. Wang, et al., Schisandrin B mitigates hepatic steatosis and promotes fatty acid oxidation by inducing autophagy through AMPK/mTOR signaling pathway, Metabolism 131 (2022) 155200, https://doi.org/10.1016/j.metabol.2022.155200.

[41] C. Huang, Q. Yong, Y. Lu, L. Wang, Y. Zheng, L. Zhao, et al., Gentiopicroside improves non-alcoholic steatohepatitis by activating PPARα and suppressing HIF1, Front. Pharmacol. 15 (2024) 1335814, https://doi.org/10.3389/fphar.2024.1335814.

[42] C.Y. Fan, J. Pan, N. Usuda, A.V. Yeldandi, M.S. Rao, J.K. Reddy, Steatohepatitis, spontaneous peroxisome proliferation and liver tumors in mice lacking peroxisomal fatty acyl-CoA oxidase. Implications for peroxisome proliferator-activated receptor alpha natural ligand metabolism, J. Biol. Chem. 273 (25) (1998) 15639–15645, https://doi.org/10.1074/jbc.273.25.15639.

[43] D. Lu, A. He, M. Tan, M. Mrad, A. El Daibani, D. Hu, et al., Liver ACOX1 regulates levels of circulating lipids that promote metabolic health through adipose remodeling, Nat. Commun. 15 (1) (2024) 4214, https://doi.org/10.1038/s41467-024-48471-2.

[44] A. He, X. Chen, M. Tan, Y. Chen, D. Lu, X. Zhang, et al., Acetyl-CoA derived from hepatic peroxisomal β-oxidation inhibits autophagy and promotes steatosis via mTORC1 activation, Mol. Cell. 79 (1) (2020) 30–42, https://doi.org/10.1016/j.molcel.2020.05.007.
[45] L. Ding, W. Sun, M. Balaz, A. He, M. Klug, S. Wieland, et al., Peroxisomal β-oxidation acts as a sensor for intracellular fatty acids and regulates lipolysis, Nat. Metab. 3 (12) (2021) 1648–1661, https://doi.org/10.1038/s42255-021-00489-2.
[46] A.S. Divakaruni, W.Y. Hsieh, L. Minarrieta, T.N. Duong, K.K.O. Kim, B.R. Desousa, et al., Etomoxir inhibits macrophage polarization by disrupting coa homeostasis, Cell Metabol. 28 (3) (2018) 490–503, https://doi.org/10.1016/j.cmet.2018.06.001.
[47] B. Zierfuss, A. Buda, A. Villoria-González, M. Logist, J. Fabjan, P. Parzer, et al., Saturated very long-chain fatty acids regulate macrophage plasticity and invasiveness, J. Neuroinflammation 19 (1) (2022) 305, https://doi.org/10.1186/s12974-022-02664-y.
[48] S. Russo, M. Kwiatkowski, N. Govorukhina, R. Bischoff, B.N. Melgert, Meta-inflammation and metabolic reprogramming of macrophages in diabetes and obesity: the importance of metabolites, Front. Immunol. 12 (2021) 746151, https://doi.org/10.3389/fimmu.2021.746151.
[49] T. Sidiq, A. Khajuria, P. Suden, R. Sharma, S. Singh, K.A. Suri, et al., Possible role of macrophages induced by an irridoid glycoside (RLJ-NE-299A) in host defense mechanism, Int. Immunopharm. 11 (1) (2011) 128–135, https://doi.org/10.1016/j.intimp.2010.10.017.
[50] S. Zeng, D. Wang, Y. Cao, N. An, F. Zeng, C. Han, et al., Immunopotentiation of Caffeoyl Glycoside from Picrorhiza scrophulariiflora on activation and cytokines secretion of immunocyte in vitro, Int. Immunopharm. 8 (12) (2008) 1707–1712, https://doi.org/10.1016/j.intimp.2008.07.016.
[51] X. Yang, W. Gao, B. Wang, X. Wang, H. Guo, Y. Xiao, et al., Picroside II inhibits RANKL-mediated osteoclastogenesis by attenuating the NF-κB and MAPKs signaling pathway in vitro and prevents bone loss in lipopolysaccharide treatment mice, J. Cell. Biochem. 118 (12) (2017) 4479–4486, https://doi.org/10.1002/jcb.26105.
[52] W. Sheng, G. Ji, L. Zhang, Role of macrophage scavenger receptor MSR1 in the progression of non-alcoholic steatohepatitis, Front Immunol. 13 (2022) 1050984, https://doi.org/10.3389/fimmu.2022.1050984.
[53] O. Govaere, S.K. Petersen, N. Martinez-Lopez, J. Wouters, M. Van Haele, R.M. Mancina, et al., Macrophage scavenger receptor 1 mediates lipid-induced inflammation in non-alcoholic fatty liver disease, J. Hepatol. 76 (5) (2022) 1001–1012, https://doi.org/10.1016/j.jhep.2021.12.012.